Theoretical simulations of the He 79 Br 2 B, v=8X, v =0 excitation spectrum: Spectroscopic manifestation of a linear isomer?

Marta I. Hernández, Tomás González-Lezana, Gerardo Delgado-Barrio, Pablo Villarreal, and Alexei A. Buchachenko

Citation: The Journal of Chemical Physics **113**, 4620 (2000); doi: 10.1063/1.1288793
View online: http://dx.doi.org/10.1063/1.1288793
View Table of Contents: http://scitation.aip.org/content/aip/journal/jcp/113/11?ver=pdfcov
Published by the AIP Publishing

Theoretical simulations of the $He^{79}Br_2$ B, $v=8\leftarrow X$, $v''=0$ excitation spectrum: Spectroscopic manifestation of a linear isomer?

Marta I. Hernández, Tomás González-Lezana, Gerardo Delgado-Barrio, Pablo Villarreal,[a] and Alexei A. Buchachenko[b]
Instituto de Matemáticas y Física Fundamental, C.S.I.C., Serrano 123, Madrid 28006, Spain

(Received 23 February 2000; accepted 21 June 2000)

Possible manifestations of a linear isomer of a rare gas–halogen molecule van der Waals complex in its $B\leftarrow X$ excitation spectrum are analyzed using a continuous one-parametric family of X-state potential energy surfaces (PESs) with variable depths of minima in the T-shaped and linear configurations. For the $HeBr_2$ complex as an example, the propensities in the frequencies and intensities of the representative transitions from T-shaped and linear isomers are analyzed and the variation of the whole spectrum with the topology of the X-state PES is established. Qualitatively good agreement with the experimental $HeBr_2$ spectrum clearly suggests that the unassigned secondary band of the observed spectrum is likely formed by transitions from the linear isomer, whose energy is very close to that of the T-shaped one. Present results provide strong evidence for the possibility to detect a linear isomer of rare gas–halogen molecule complexes via conventional excitation spectroscopy. © *2000 American Institute of Physics.* [S0021-9606(00)01135-1]

I. INTRODUCTION

During almost three decades, van der Waals (vdW) complexes of halogen molecules with rare gas atoms RgX_2 have attracted an intent attention of experimentalists and theoreticians. Very recent reviews of Janda and co-workers[1,2] clearly demonstrate why these systems have become one of the important ''paradigms'' of the theory of vdW bonding: their apparent simplicity contradicts the complexity of their interaction potential energy surfaces (PESs), spectroscopy, and decay dynamics.

One of the most interesting problems is the topology of their ground-state PES. Apart from several interhalogen complexes RgXY (ArClF, KrClF, HeClF, and ArICl), whose linear structure was established by means of microwave spectroscopy,[3–6] a triangular structure of the RgX_2 complexes in the ground X and electronically-excited B states fits almost all available experimental data.[1,2] Interpretation of only few experimental observations [one-atom cage effect in $ArI_2(B)$ complex,[7–12] two separate progressions in the Rydberg state excitation, and ionization spectra of ArI_2 and KrI_2,[13,14] some features of total $Rg+Cl_2$ scattering cross sections][15–17] implies the existence of a linear isomer. On the other hand, all high-level *ab initio* calculations[18–35] and semiempirical multiproperty analysis based on *ab initio* data[25,30,31,34] have consistently revealed that the ground-state PES has minima in both triangular and linear configurations (hereafter T-shaped and linear minima) and the latter is predicted to be the deepest one. It was shown by Huang *et al.* that it is the zero-point vibrational energy responsible for stabilization of the T-shaped isomer: the ground vdW vibrational level $n_X=0$ corresponds to the secondary T-shaped minimum but not to the ground linear well.[26] This finding (see also Refs. 1, 2, 30, 34) and the well-established T-shaped structure of the complexes in the B state explain *why* the excitation spectroscopy probes the T-shaped isomer. However, the question still remains *how* the linear isomer could be detected. In this respect, theory may provide very useful hints identifying those features of spectra and dynamics which are hardly interpreted in terms of a T-shaped structure.

The main goal of the present work is to get insight into the dependence of the features of the $B\leftarrow X$ excitation spectrum on the shape of the ground-state PES. For this purpose, we construct, using a sort of diatomics-in-molecule approximation, a one-parametric family of PESs which undergo the evolution from the single T-shaped topology to the situation when the linear minimum has the lowest energy.

This model is applied to the $HeBr_2$ complex. The $B\leftarrow X$ excitation spectrum recorded by Jahn *et al.*[36] for the vibrational excitation of the $Br_2(B)$ fragment $v=8$ consists of a main peak shifted by 3.72 cm^{-1} to the blue from the B, $v=8\leftarrow X$, $v''=0$ band of the bare Br_2 molecule. Partially resolved rotational structure of the peak corresponds to transitions between the ground vdW vibrational levels $n_X=n_B=0$ of the T-shaped complex. A unique feature of the $HeBr_2$ spectrum is the presence of a secondary band shifted by 5–6 cm^{-1} further to the blue. It has a complicated structure and an intensity ca. 4–5 times lower than that of the main peak. The secondary feature was tentatively assigned to transitions to the excited $n_B=1$ vdW level of the B state.[36] Accompanied theoretical simulations for $n_B=1\leftarrow n_X=0$ transitions matched the observed blue shift of the secondary feature, but barely underestimated its intensity. The same inconsistency was obtained in our calculations despite very impressive

[a]Author to whom correspondence should be addressed; electronic mail: pablo@fam88.imaff.csic.es
[b]On sabbatical leave from the Laboratory of Molecular Structure and Quantum Mechanics, Department of Chemistry, Moscow State University, Moscow 119899, Russia.

agreement with experimental data on the vibrational predissociation dynamics[36–38] achieved even at high v's, where the intramolecular vibrational relaxation causes extreme sensitivity of the dynamics to the properties of the PESs.[39–42]

We try to assign these two spectrum features to transitions from the distinct isomers having similar energies. Implementing the family of the ground-state PESs and comparing the simulated spectra with the observed one, we aim to support a new assignment which involves the coexistence of T-shaped and linear isomers and deduce the qualitative estimation of their energies which can be compared with available *ab initio* data.[27,36]

II. POTENTIAL ENERGY SURFACES

A. *B* state

For the B state we use so-called IDIM PT1 PES[43–45] from Ref. 42, the best available one at least for spectroscopy and predissociation dynamics of the $HeBr_2$ complex for a large range of v's. It has the following analytical form:

$$V_B=\frac{1}{4}\sum_{\alpha=a,b}\{3V_{\Pi}(R_\alpha)+V_{\Sigma}(R_\alpha) -[V_{\Pi}(R_\alpha)-V_{\Sigma}(R_\alpha)]\cos^2\beta_\alpha\}, \quad (1)$$

where $\alpha=a,b$ enumerates bromine atoms, R_α are the He–Br distances, and β_α are the angles between Br_2 axis $\mathbf{r}$ and $\mathbf{R}_\alpha$. V_Λ are the potentials of the HeBr diatomic molecule in the $^2\Sigma^+$ and $^2\Pi$ electronic states. Their parameters are given in Ref. 42. In the calculations Jacobi coordinates (r,R,θ) were used, where r is the Br–Br distance, R is the distance between Br_2 center-of-mass and He atom, and θ is the angle between $\mathbf{r}$ and $\mathbf{R}$.

The IDIM PT1 PES has a primary T-shaped well and a very shallow long-range linear minimum.[42] Another B-state PES used here, the empirical Morse pairwise (EMP),[39] is almost the same in the vicinity of the T-shaped minimum but has no linear well.

B. *X* state

Our model for X-state PESs also originates from the IDIM PT1 approach. The latter utilizes the asymptotic Hund case (c) electronic wave functions of the halogen molecule to approximate interaction PES by first-order perturbation theory. It was noted[43,44] that there are two such functions of 0_g^+ symmetry correlating to the ground $^2P_{3/2}+{}^2P_{3/2}$ dissociation limit. In terms of $|jm\rangle_\alpha$ functions of bromine atoms, they can be expressed as[43,44,46]

$$\phi_1=\left[\left|\frac{3}{2}\frac{3}{2}\right\rangle_a\left|\frac{3}{2}-\frac{3}{2}\right\rangle_b-\left|\frac{3}{2}-\frac{3}{2}\right\rangle_a\left|\frac{3}{2}\frac{3}{2}\right\rangle_b\right]\Big/\sqrt{2},$$

$$\phi_2=\left[\left|\frac{3}{2}\frac{1}{2}\right\rangle_a\left|\frac{3}{2}-\frac{1}{2}\right\rangle_b-\left|\frac{3}{2}-\frac{1}{2}\right\rangle_a\left|\frac{3}{2}\frac{1}{2}\right\rangle_b\right]\Big/\sqrt{2}.$$

Any normalized linear combination of these functions can be taken as an asymptotic eigenfunction for the ground $X0_g^+$ state. Depending on the particular choice, the IDIM PT1 model gives distinct interaction PESs, including those having two minima. The evident weakness of IDIM PT1 model to predict a unique well-defined X-state PES can be turned into an advantage for constructing a smoothly varying family of PESs.

Linear combination of ϕ_1 and ϕ_2 with a mixing angle ξ, $\Psi_X(\xi)=\phi_1\cos\xi-\phi_2\sin\xi$, leads to the following analytical expression of the PES:

$$V_X(\xi)=\sum_{\alpha=a,b}\{V_{\Pi}(R_\alpha)(5-2\cos^2\xi)/6+V_{\Sigma}(R_\alpha) \times(2\cos^2\xi+1)/6 -\tfrac{1}{2}[V_{\Pi}(R_\alpha)-V_{\Sigma}(R_\Sigma)]\cos 2\xi\cos^2\beta_\alpha\}. \quad (2)$$

It should be noted that the mixing between individual wave functions is an important ingredient of the more elaborate and accurate diatomics-in-molecule approaches by Grigorenko *et al.*[47] and Naumkin.[48] Still, however, the model is oversimplified to give quantitative results being parametrized by true HeBr potentials. It is possible, however, to choose them *ad hoc* in order to let the family of $V_X(\xi)$ PES cover a wide range of relative depths of T-shaped and linear potential wells. V_Σ and V_Π were represented by Morse functions

$$V_\Lambda=\lambda(\xi)D_\Lambda^0\{\exp[-2\alpha_\Lambda(R-\overline{R}_\Lambda)]-2 \times\exp[-\alpha_\Lambda(R-\overline{R}_\Lambda)]\}, \quad (3)$$

where the parameters $\overline{R}_\Lambda=3.81$ Å and $\alpha_\Lambda=1.55$ Å^{-1} for both $\Lambda=\Sigma,\Pi$ were borrowed from the X-state EMP potential,[39] while dissociation energies was taken as $D_\Sigma^0=40\ \mathrm{cm}^{-1}$, $D_\Pi^0=4\ \mathrm{cm}^{-1}$. The scaling factor $\lambda(\xi)$ was introduced in Eq. (3) in order to compensate for the changes of interaction strength with ξ. For each value of ξ, it was adjusted so that the energy of the ground vdW level for $V_X(\xi)$ PES is equal to that obtained with the X-state EMP potential. This adjustment was performed within rotational infinite order sudden approximation (see, e.g., Ref. 49), so that the accurate energies of $n_X=0$ levels are systematically higher[50] by ca. 0.3 cm^{-1}. No further refinement of the $V_X(\xi)$ PESs was attempted.

Positions and depths of the minima on selected $V_X(\xi)$ PESs are listed in Table I. At small values of ξ, the PES has a single T-shaped minimum, while at ξ between 40° and 50°, a shallow secondary linear well appears. Its depth rapidly increases and approaches almost the same value as that of the T-shaped well at $\xi=66.5°$ and 67.5°. As we will show later, this situation is the most interesting in the present context. Further increase makes the linear minimum global, reducing the depth of the T-shaped well. Hence, Eq. (3) provides a desirable one-parametric family of PESs with a smooth transition from a global T-shaped to a linear structure at constant energy of the ground vibrational level. The topology of EMP[39] and *ab initio* based PESs[36,27] is also characterized in Table I.

For better correspondence with the results of rovibrational energy level calculations it is worth also to characterize the ''diabatic'' PESs, i.e., two-dimensional potentials averaged over r with proper Br_2 vibrational wave functions. The contour plots of selected diabatic PESs for X, $v''=0$ and

TABLE I. Positions R_e and depths D_e of the *T*-shaped and linear minima on the adiabatic ground-state $HeBr_2$ PESs at the equilibrium Br_2 distance 1.988 Å.

		T-shaped		Linear	
PES	λ	R_e, Å	D_e, cm^{-1}	R_e, Å	D_e, cm^{-1}
$V_X(0°)$	0.950	3.64	38.74	⋯	⋯
$V_X(20°)$	0.999	3.64	38.69	⋯	⋯
$V_X(40°)$	1.149	3.64	38.52	⋯	⋯
$V_X(60°)$	1.382	3.63	38.16	4.93	32.17
$V_X(65°)$	1.442	3.63	38.00	4.93	36.17
$V_X(66.5°)$	1.458	3.63	37.94	4.93	37.31
$V_X(67.5°)$	1.468	3.63	37.87	4.93	38.04
$V_X(70°)$	1.464	3.63	37.02	4.93	39.03
$V_X(80°)$	1.375	3.62	32.67	4.93	39.67
$V_X(90°)$	1.345	3.62	31.26	4.93	39.85
EMP[a]		3.64	39.62	⋯	⋯
Scaled MP4[b]		3.70	40.21	4.50	44.11
MP4[c]		3.70	38.5	4.50	42.8

[a]Reference 39.

[b]The PES obtained from the *ab initio* fourth order Møller–Plesset $HeCl_2$ PES by adjusting the equilibrium distance and depth of the linear minimum (Ref. 36).

[c]*Ab initio* fourth-order Møller–Plesset calculations (Ref. 27). Quoted values were borrowed from Ref. 1.

B, $v=8$ in Cartesian coordinates $x=R\cos\theta$ and $y=R\sin\theta$ are presented in Fig. 1. IDIM PT1 and EMP *B*-state PESs are very similar, whereas $V_X(67.5°)$ and EMP *X*-state PESs differ in the linear configuration.

III. SIMULATIONS OF EXCITATION SPECTRUM

The rotational energy levels of the $HeBr_2$ complex are classified by $J^{p_i p_j}$ quantum numbers, where J is the total rotational angular momentum quantum number, and p_i, p_j are the parities with respect to inversion of nuclear coordinates and exchange of Br nuclei, respectively.[41,49] The sign of p_j defines which rotational angular momenta of the Br_2 fragment j, even or odd, contribute to the total wave function of the complex. In what follows we will designate the rotational levels $J^{p_i p_j}$ as t'' and t for the *X* and *B* electronic states, respectively.

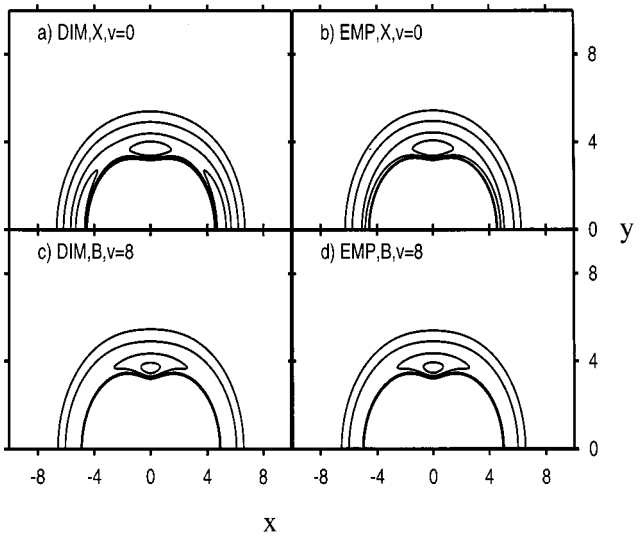

FIG. 1. Contour plots of the diabatic PESs averaged over the Br_2 vibrational wave functions: (a) *X*-state $V_X(67.5°)$, (b) *X*-state EMP, (c) *B*-state IDIM PT1, (d) *B*-state EMP. Contour lines correspond to the energies −30, −20, −10, and −5 cm^{-1}.

Total excitation cross section for the B, $v\leftarrow X,v'',n_X$ transition at photon energy E and internal temperature of the complex T is expressed as

$$\sigma(B,v\leftarrow X,v'',n_X;E;T) = \sum_t \sum_{t''} \sum_{n_B} w_X(T) g_{t''} \sigma(B,v,n_B,t\leftarrow X,v'',n_X,t'';E), \tag{4}$$

where $w_X(T)$ is a Boltzmann factor accounting for the population of initial level, $g_{t''}$ is the statistical factor accounting for the nuclear spin $I=3/2$ of ^{79}Br nuclei and equal to 5/8 or 3/8 for $p_j''=-1$ or $+1$, respectively, and $\sigma(B,v,n_B,t\leftarrow X,v'',n_X,t'';E)$ is the excitation cross section for a single rotational transition. The B, $v\neq 0$ states of the complex are metastable due to the vibrational predissociation. Assuming separation between the metastable levels, one can use a discrete–discrete version to approximate the excitation cross sections,[49]

$$\sigma(B,v,n_B,t\leftarrow X,v'',n_X,t'';E) \approx I(B,v,n_B,t\leftarrow X,v'',n_X,t'';E_0)\,\frac{\Gamma_0/2\pi}{(E-E_0)^2+(\Gamma_0/2)^2}, \tag{5}$$

where E_0 is the transition energy and Γ_0 is the predissociation width of the B, v, n_B, t energy level. The intensity factor is the matrix element of the transition dipole moment operator. Its explicit form can be found in Refs. 41, 51, 52. The transition dipole moment vector was taken to be parallel to the *r* axis. The (unknown) electronic transition dipole moment function was assumed to be constant since its dependence on *R* should be weak, while the dependence on *r* is not important for the transitions to the same v level considered here. The nuclear energies and wave functions were calculated variationally, while the diabatic Fermi Golden rule approach was implemented for predissociation widths. Computational parameters were chosen to be the same as in our previous works.[39,41]

A. Vibrational energy levels

The lowest vdW vibrational level patterns of $HeBr_2$ at $J=0$ belong to two symmetry blocks, $t=0^{++}$ and 0^{+-}. For the 0^{++} levels of the *B* state, Golden rule calculations with IDIM PT1 PES yield −13.761, −7.389 cm^{-1}, and 0.013, 0.032 cm^{-1} for energies and halfwidths of $n_B=0$, 1 levels, respectively. The *X*-state energy levels calculated with $V_X(\xi)$ PESs for both parity blocks are listed in Table II. They were assigned to T-shaped or linear isomers. For the latter, the levels of opposite p_j parity form doublets which can be interpreted in terms of tunneling splitting in the effective angular double-well potential. They appear as excited bending levels $n_X=1$ (0^{++} block) of the complex at $\xi<60°$. Their energy and splitting rapidly decrease with ξ and, between $\xi=67.5°$ and 70°, they become the ground levels of the com-

TABLE II. Lowest van der Waals energy levels of the $HeBr_2$ complex (cm^{-1}) computed with $V_X(\xi)$ PESs for $J=0$. Parity with respect to exchange of the Br nuclei p_j is indicated in parentheses. The energies given in *italic* correspond to the linear potential well.

ξ				
0°	−17.2781 (+)	−10.0337 (−)	−6.2854 (+)	−3.0196 (−)
40°	−17.2834 (+)	−10.7476 (−)	−8.0033 (+)	−6.2925 (−)
50°	−17.2877 (+)	−13.4456 (−)	−9.9558 (+)	−8.1049 (−)
60°	−17.2894 (+)	*−13.7239 (−)*	*−13.6167 (+)*	−11.4374 (−)
65°	−17.2709 (+)	*−15.8397 (−)*	*−15.7939 (+)*	−12.0173 (−)
66.5°	−17.2651 (+)	*−16.4837 (−)*	*−16.4312 (+)*	−12.1812 (−)
67.5°	−17.2722 (+)	*−16.8980 (−)*	*−16.8162 (+)*	−12.2829 (−)
70°	*−17.4344 (+)*	*−17.4126 (−)*	−16.6417 (+)	−12.1517 (−)
90°	*−17.4882 (+)*	*−17.4874 (−)*	−13.1254 (+)	−10.5393 (−)

plex. This happens at a higher value of ξ than the inversion of the depths of T-shaped and linear minima (see Table I) due to the higher zero-point vibrational energy of the linear isomer.[26] In the limiting case $\xi=90°$, the energy of linear isomer is ca. 4 cm^{-1} lower than that of the T-shaped one and the tunneling splitting becomes negligible.

Cartesian contour plots of the probability density distributions for the *B*- and *X*-state levels are depicted in Figs. 2 and 3 for diatomics-in-molecule and EMP PESs, respectively. The density distributions for $n_B=0$ are almost identical for both potentials, whereas the $n_B=1$ wave function is markedly more extended toward the linear configuration for IDIM PT1 PES. The probability density distributions for 0^{++} $n_X=0$, 1 levels calculated with the $V_X(67.5°)$ and EMP PESs are dramatically different. Despite the $V_X(67.5°)$ $n_X=0$ wave function is still localized in the T-shaped well, it extends remarkably to the linear configuration, whereas the $n_X=1$ wave function corresponds to the linear well (the maxima of probability density distribution are shifted to nonzero angles due to the sin θ Jacobian).

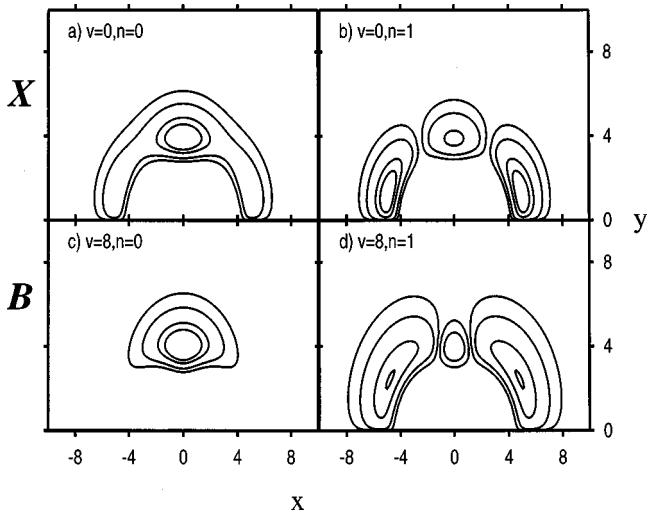

FIG. 2. Contour plots of the probability density distributions for the $v''=0$ and $v=8$ vdW levels calculated with $V_X(67.5°)$ and IDIM PT1 PESs. (a) $n_X=0$, (b) $n_X=1$, (c) $n_B=0$, (d) $n_B=1$. Contour lines correspond to 0.25, 0.1, 0.01, and 0.001.

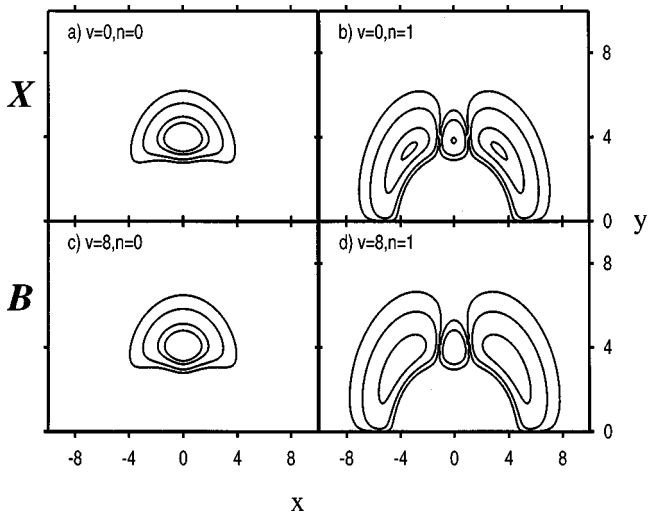

FIG. 3. Same as Fig. 2, but for EMP PESs.

B. Four-state model for excitation spectrum

For qualitative interpretation of the complete spectrum, it is worth to consider a simple spectrum model which takes into account the transitions between the lowest four vdW levels $n_X=0$, 1 and $n_B=0$, 1 for a single rotational transition, for example, $0^{++}\leftarrow 1^{--}$, a quite representative one.[39]

Each $[n_B\leftarrow n_X]$ transition is characterized by a blue shift $\Delta\omega$ with respect to the bare Br_2 *B*, $v=8\leftarrow X$, $v''=0$ transition, equal to the energy difference between the final and initial vdW levels, and intensity *I* taken from Eq. (5). Neither the statistical weight nor the Boltzmann factor are included. Shifts and intensities are listed in Table III for various *X*- and *B*-state PESs. Note that for the same *B*-state PES the shifts of the $[0\leftarrow 0]$ and $[1\leftarrow 0]$ transitions are almost the same for all $V_X(\xi)$ PESs which maintain a constant energy for the $n_X=0$ level [within an uncertainty in the adjustment of λ parameter in Eq. (3)].

Table III gives clear evidence for the strong variation of the transition blue shifts and intensities with the ξ parameter, i.e., with the topology of the $V_X(\xi)$ PES. The purely T-shaped $V_X(0^0)$ PES is very close to the EMP one and the intensity ratios for different transitions can be clearly understood in terms of the overlaps of the corresponding wave functions. According to Fig. 3, ''diagonal'' $n_X=n_B$ transitions should be much more intense than the ''nondiagonal'' ones, $n_X\neq n_B$. This is indeed the case. In addition, the second diagonal $[1\leftarrow 1]$ transition appears to be much weaker than the first one $[0\leftarrow 0]$. The intensities of all transitions change only slightly when ξ increases up to 60°. At this point, $n_X=1$ level starts to represent a linear isomer. This leads to a sudden increase of both shift and intensity of the $[1\leftarrow 1]$ transition due to favorable overlap with the $n_B=1$ wave function which markedly extends towards the linear configuration (Fig. 2). In contrast, the overlap with $n_B=0$ state becomes less favorable and the intensity of $[0\leftarrow 1]$ transitions decreases. Further increase of ξ leads to some spreading of the probability density distribution of the n_X levels. As a result, intensities of the nondiagonal transitions increase, while those of the diagonal ones slightly decrease.

TABLE III. Blue shifts $\Delta\omega$ (cm^{-1}) and intensities I of the B, $v=8$, n_B, $1^{--}\leftarrow X$, $v''=0$, n_X, 0^{++} transitions for n_X, $n_B=1,0$. Transitions given in *italic* corresponds to the linear isomer.

		0←0		1←0		0←1		1←1	
PES X	PES B	$\Delta\omega$	I	$\Delta\omega$	I	$\Delta\omega$	I	$\Delta\omega$	I
EMP	EMP	3.721	2.7(−5)	11.148	2.5(−9)	−2.932	5.1(−8)	4.495	5.7(−7)
EMP	IDIM PT1	3.811	2.7(−5)	10.183	4.5(−9)	−2.842	5.7(−8)	3.530	5.1(−6)
$V_X(0°)$	EMP	3.280	2.7(−5)	10.707	2.6(−8)	−4.163	6.0(−8)	3.264	1.9(−7)
$V_X(0°)$	IDIM PT1	3.370	2.7(−5)	9.742	2.6(−8)	−4.073	6.3(−8)	2.299	1.3(−7)
$V_X(40°)$	IDIM PT1	3.375	2.7(−5)	9.747	6.3(−9)	−3.380	5.7(−8)	2.992	3.3(−7)
$V_X(60°)$	IDIM PT1	3.382	2.7(−5)	9.753	2.6(−8)	*−0.235*	*2.1(−8)*	*6.136*	*1.9(−5)*
$V_X(65°)$	IDIM PT1	3.362	2.6(−5)	9.733	2.1(−7)	*1.930*	*2.3(−7)*	8.301	*1.7(−5)*
$V_X(66.5°)$	IDIM PT1	3.355	2.6(−5)	9.726	6.6(−7)	*2.568*	*8.4(−7)*	*8.939*	*1.6(−5)*
$V_X(67.5°)$	IDIM PT1	3.361	2.3(−5)	9.732	2.6(−6)	*2.953*	*3.7(−6)*	*9.324*	*1.4(−5)*
$V_X(70°)$	IDIM PT1	*3.558*	*9.6(−7)*	*9.929*	*1.5(−5)*	2.744	2.6(−5)	9.115	3.3(−7)
$V_X(90°)$	IDIM PT1	*3.617*	*4.8(−8)*	*9.988*	*1.4(−5)*	−0.516	6.0(−6)	5.855	6.3(−7)
$V_X(90°)$	EMP	*3.526*	*4.2(−8)*	*10.953*	*9.6(−6)*	−0.607	6.0(−6)	6.820	7.8(−7)

The $n_X=1$ level of linear isomer gets closer in energy to the $n_X=0$ of T-shaped isomer and the shifts of the corresponding transitions become comparable. At $\xi=67.5°$, $n_X=0$ and 1 levels are almost degenerated. Calculated transitions intensities are again in good accord with the overlap of the vibrational wave functions (see Fig. 2). The second sudden change occurs between $\xi=67.5°$ and 70° when the linear isomer acquires lower energy than the T-shaped ones, i.e., $n_X=0$ level corresponds to the linear minimum, while $n_X=1$ to the T-shaped one. The intensities of the diagonal transitions fall off by almost two orders-of-magnitude, but the nondiagonal transitions become one order-of-magnitude stronger. The energy of $n_X=1$ level increases and the shifts of associated transitions decrease again.

Some results obtained with EMP X- and B-state PESs are also presented in Table III. They demonstrate, first, that the transition intensities do not depend significantly on what T-shaped PES, EMP, or $V_X(0^0)$ is used for the X-state. Second, they show that the existence of the linear minimum on the B-state PES neither affects the transition intensities: even for the extreme case of $V_X(90°)$ PES, intensities calculated with IDIM PT1 and EMP PESs are not far from each other.

We used the four-state model also to check the discrete–discrete approximation to the excitation spectrum. Rigorous discrete–continuum (or lineshape)[49] calculations were performed for the $V_X(67.5°)$ IDIM PT1 pair of PESs as described elsewhere.[39,41] In this case the shifts and integrated intensities of individual transitions were determined from the continuous excitation profile using Lorentzian fits to the corresponding peaks. As is seen in Fig. 4, the agreement between both approaches is excellent despite minor discrepancy more evident for the transitions to the $n_B=1$ level. This proves that at low v's the discrete–discrete approximation works very well not only for shifts and widths,[39,41] but also for transition intensities.

C. Rotationally resolved excitation spectrum simulations

More realistic simulations of the B, $v=8\leftarrow X$, $v''=0$ spectrum were performed within the discrete–discrete approximation. For each set of t'' and t rotational quantum numbers, variational energies and wave functions of the five lowest vdW n_X and n_B levels were used to determine blue shifts and intensities $I(B,v,n_B,t\leftarrow X,v'',n_X,t'';E_0)$. The resulting sticky spectrum was dressed by Lorentzian functions [Eq. (5)] with a common halfwidth $\Gamma_0/2=0.023\,cm^{-1}$, the average value for $n_B=0$ and 1 levels at $J=0$. It was checked that this assumption does not alter the spectrum significantly. Equation (4) was used to evaluate the full excitation profile at the internal temperature of 1.6 K established in our previous analysis.[41] It was found that it is sufficient to consider transitions with $J''\leqslant 4$. Around 1100 transitions were taken into account for each pair of X, B PESs.

Spectra obtained with selected $V_X(\xi)$ and IDIM PT1

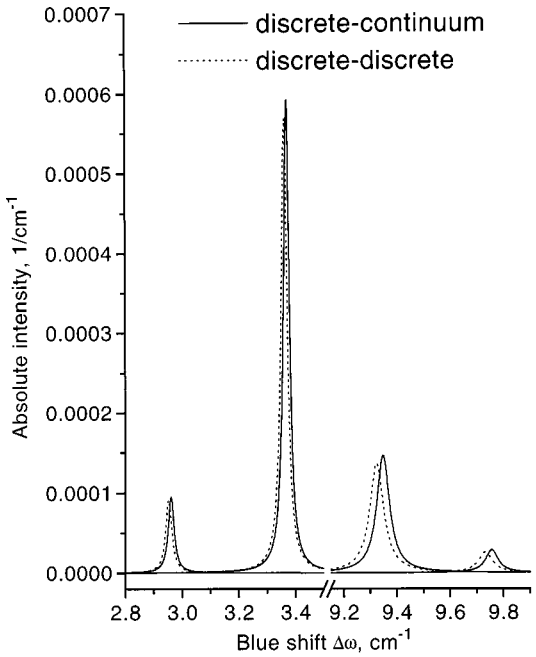

FIG. 4. Excitation cross-sections for $HeBr_2B$, $v=8$, n_B, $0^{++}\leftarrow X$, $v''=0$, n_X, 1^{--} transitions calculated using discrete–continuum line shape approach (solid line) and simulated within discrete–discrete approximation (dashed line) for $V_X(67.5°)$ and IDIM PT1 PESs. The peaks, from left to right, correspond to $n_B=0\leftarrow n_X=1$, $n_B=0\leftarrow n_X=0$, $n_B=1\leftarrow n_X=1$, and $n_B=1\leftarrow n_X=0$ transitions.

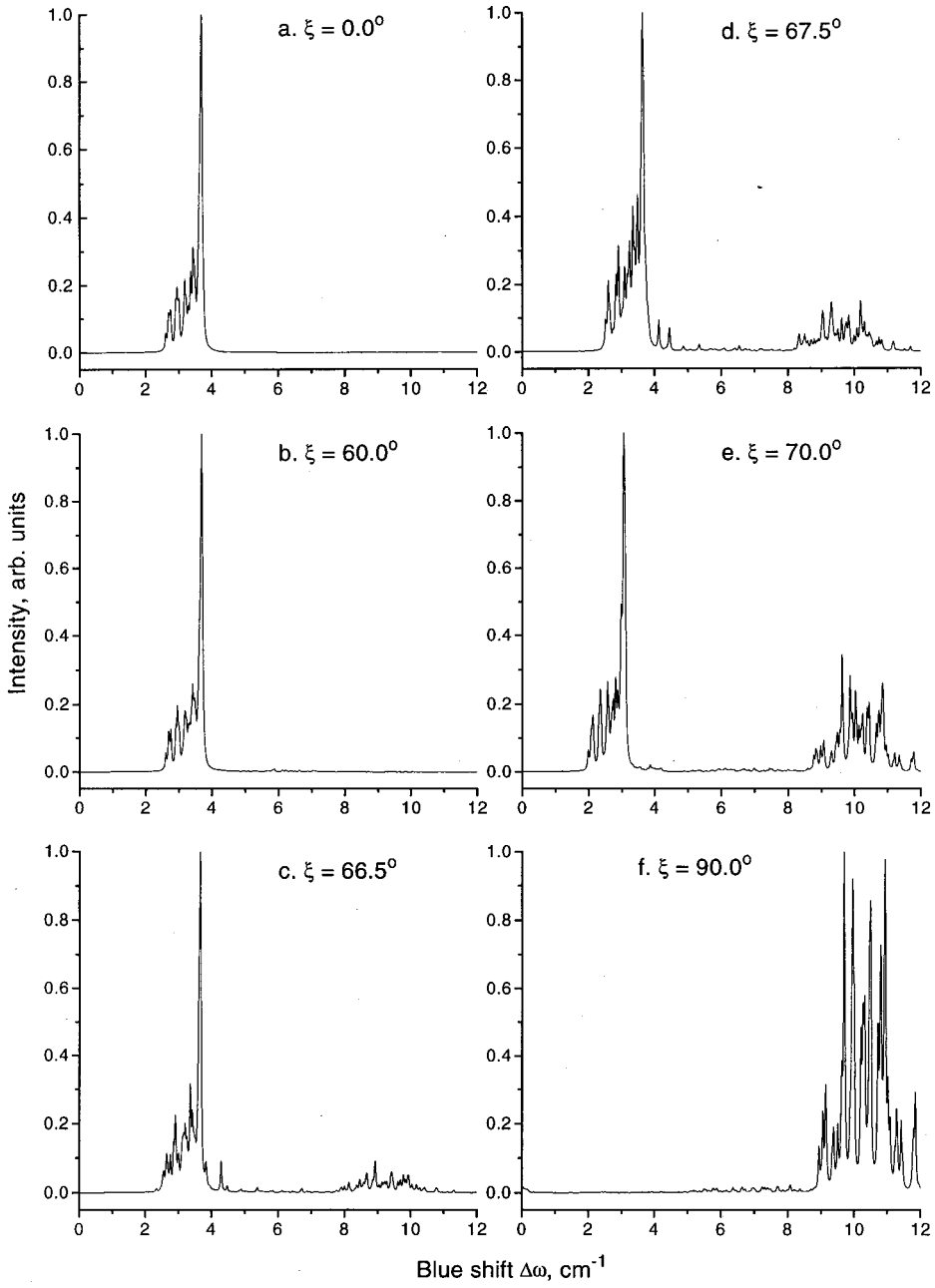

FIG. 5. $HeBr_2B$, $v=8\leftarrow X$, $v''=0$ excitation spectra simulated using selected $V_X(\xi)$ and IDIM PT1 PESs. The intensity is normalized to unity at the maximum.

PESs are shown in Fig. 5. For ξ from 0° to 60°, the spectrum consists of a single peak whose structure is typical for T-shaped complexes. It is formed exclusively by various $[0\leftarrow 0]$ rotational transitions. The transitions with $n_X \neq n_B$ have too low excitation probability (as in Table III), while the transitions $n_X=n_B\neq 0$ are suppressed due to the low population of initial levels. At $\xi=66.5°$ [Fig. 5(c)], a weak feature appears at 8–10 cm^{-1} blue shift. In agreement with the four-state model, it corresponds to $[1\leftarrow 1]$ transitions from the linear isomer. At $\xi=67.5°$ [Fig. 5(d)], the intensity of the secondary feature gets larger. Figure 6 demonstrates the $\xi=67.5°$ spectra simulated separately for the transitions from T-shaped ($n_X=0$) and linear ($n_X=1$) isomers. These simulations took into account only the two lowest vdW levels of the ground state within each symmetry block classified as belonging to the T-shaped or linear isomer. The sum of the two spectra reproduces very well the complete spectrum which includes much more transitions. In accord with the four-state model transitions from both linear $[1\leftarrow 1]$ and T-shaped $[1\leftarrow 0]$, isomers contribute to the secondary feature. Likewise, the main peak formed by the transitions from the T-shaped isomer $[0\leftarrow 0]$ contains some admixture of the linear isomer transitions $[0\leftarrow 1]$, see Table III. The intensity of the secondary feature further increases at $\xi=70°$ [Fig. 5(e)]. In the limiting case $\xi=90°$ [Fig. 5(f)], the former main peak completely disappears since the transitions from the T-shaped isomer have small probability and Boltzmann factor. The former secondary feature is composed from the $[1\leftarrow 0]$ transitions of linear isomer.

Among the simulated spectra, that corresponding to

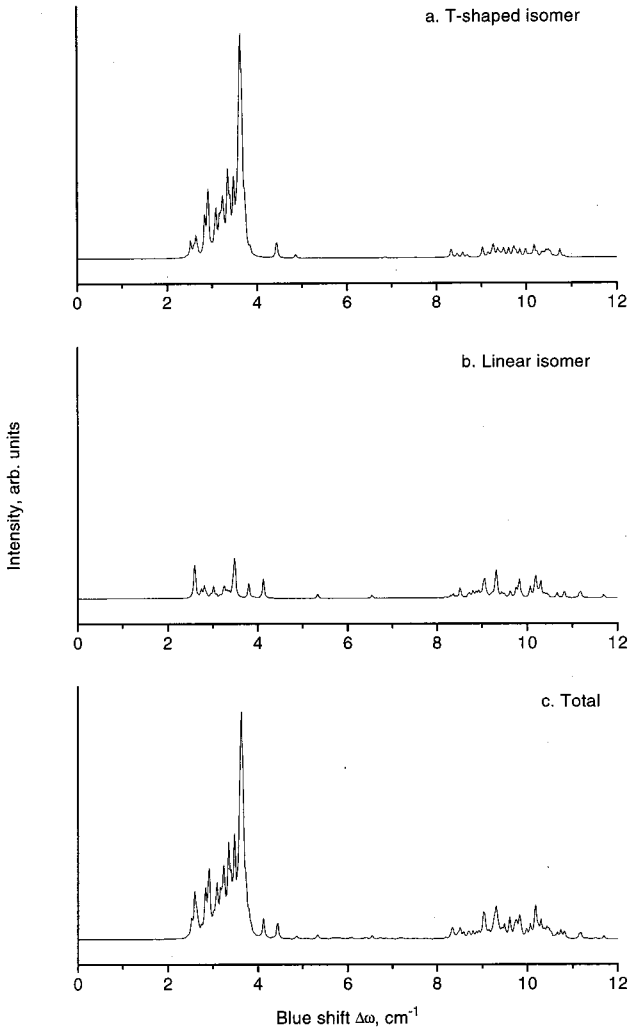

FIG. 6. Decomposition of the $HeBr_2B$, $v=8\leftarrow X$, $v''=0$ excitation spectrum simulated using $V_X(67.5°)$ and IDIM PT1 PESs: (a) and (b) spectra composed only of transitions from the lowest levels of T-shaped and linear isomers, respectively; (c) result of the complete simulations.

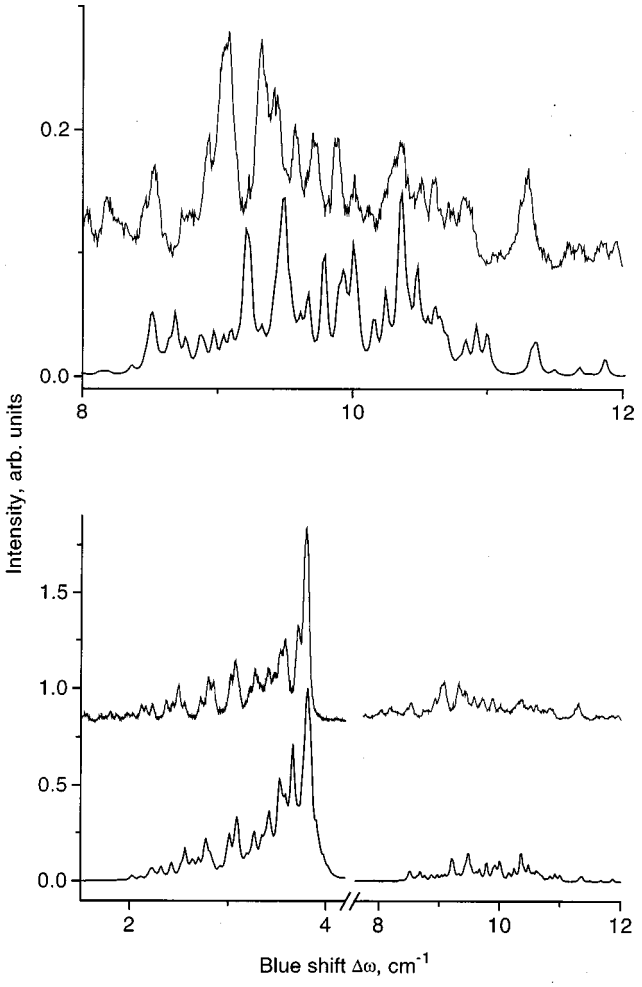

FIG. 7. Comparison of experimental (upper curve) and simulated using $V_X(67.5°)$ and IDIM PT1 PESs (lower curve) $HeBr_2B$, $v=8\leftarrow X$, $v''=0$ excitation spectra. For both spectra, intensity is normalized to unity at the maximum. Simulated spectrum is shifted by 0.16 cm^{-1}. Upper panel magnifies the secondary spectrum feature.

$V_X(67.5°)$ PES is the closest to the observed one. The whole spectra are compared on the lower panel of Fig. 7. The upper curve represents experimental spectrum from Ref. 36, while the lower is the simulated one shifted by 0.16 cm^{-1} in order to compensate for an error in the position of the maximum. As can be seen, the main peak is qualitatively well reproduced as is the intensity ratio of the two features. The upper panel of Fig. 7 magnifies the secondary feature. Its structure is rather complicated, but several similarities between the experiment and theory become apparent.

It is interesting to compare equilibrium energies of the $V_X(67.5°)$ PES with the *ab initio*-based data, in particular, with the results of fourth-order Møller–Plesset (MP4) calculations[27] given in Table I. Although *ab initio* calculations predict a larger energy difference between the two minima, it is still small enough to fit the observed spectrum if one takes into account the difference in zero-point energies and uncertainties of both *ab initio* and present approaches. Note that the latter stems not only from the qualitative nature of the model PES, but also from some assumptions made in the spectrum simulations. In particular, it would be important to understand at what extent the levels of T-shaped and linear isomers are thermally equilibrated in the supersonic beam (as we have assumed after considering their small energy difference and the low potential barrier between them).

IV. CONCLUDING REMARKS

The model developed for the ground-state potential energy surface of a rare gas atom–halogen molecule complex allows one to trace the qualitative evolution of its $B\leftarrow X$ excitation spectrum with the relative energy of T-shaped and linear isomers. Generally, the spectrum consists of two features separated approximately by the bending excitation energy of the complex in the B state. The first one is formed predominantly by the transitions from the T-shaped isomer, while the second manifests the existence of a linear isomer. If two isomers are separated in energy, only the band corresponding to the ground isomer survives due to the unfavorable overlap between the vibrational wave functions and low population. If the isomers are close enough, the two features have comparable intensities.

This model describes qualitatively well the experimental spectrum of the $HeBr_2$ complex,[36] providing strong evidence that this complex has two isomers with similar energies and that the linear isomer can really be detected using conventional $B \leftarrow X$ excitation spectroscopy. However, further efforts in both theoretical and experimental investigations are in need in order to attain a quantitative agreement.

Theoretical perspective certainly involves the implementation of more quantitative *X*-state PESs, like two existing ones, ''scaled MP4'' obtained by scaling *ab initio* MP4 PES of the $HeCl_2$ complex,[36] and *ab initio* MP4.[27,53] The former perfectly reproduces the main peak of the spectrum and the only addition to the spectrum simulations already performed in Ref. 36 to be done is the inclusion of excited vdW levels in the ground and excited states. The latter PES is a unique one which provides first-principle information on the structure and energy of the linear isomer and thus much more grounded representation of the corresponding rotational transitions should be expected.

Along the experimental avenue, it is highly desirable to gain more information on the secondary feature. The study of its variation with v and source conditions (i.e., internal temperature of the complex) will provide more solid grounds for the theoretical analysis. Our simulations also indicate the possibility of searching the linear isomer transitions at the red wing of the main peak (see Fig. 6). It will be also tempting to analyze other systems. Secondary features were detected in the $B \leftarrow X$ excitation spectra of the HeI_2, NeI_2, and ArI_2 complexes.[54–56] They were tentatively assigned to the excited *B*-state vdW levels, but at least for HeI_2 this assignment is not definitive.[1] It is of interest whether or not it is possible (and how) to detect the secondary feature for the $HeCl_2$ complex whose potentials are fairly well-known from *ab initio* calculations and multiproperty fits.[25,31,34]

ACKNOWLEDGMENTS

We thank Professor K. C. Janda for providing the experimental spectrum and encouraging discussions. This work has been supported by DGICYT (Spain) and INTAS under Grants No. PB95-0071 and No. 97-31573, respectively. A.A.B. also acknowledges the support of Spanish Ministery of Education and Culture for a sabbatical stay at CSIC.

[1] A. Rohrbacher, J. Williams, and K. C. Janda, Phys. Chem. Chem. Phys. **1**, 5263 (1999).
[2] A. Rohrbacher, N. Halberstadt, and K. C. Janda, Annu. Rev. Phys. Chem. **51**, 405 (2000).
[3] S. J. Harris, S. J. Norvick, W. Klemperer, and W. Falconer, J. Chem. Phys. **61**, 193 (1974).
[4] S. J. Norvick, S. J. Harris, K. C. Janda, and W. Klemperer, Can. J. Phys. **53**, 2007 (1975).
[5] K. Higgins, F.-M. Tao, and W. Klemperer, J. Chem. Phys. **109**, 3048 (1998).
[6] J. B. Davey, A. C. Legon, and E. R. Waclawik, Chem. Phys. Lett. **306**, 133 (1999).
[7] M. L. Burke and W. Klemperer, J. Chem. Phys. **98**, 1797 (1993).
[8] A. E. Stevens Miller, C.-C. Chuang, H. C. Fu, K. J. Higgins, and W. Klemperer, J. Chem. Phys. **111**, 7844 (1999).
[9] K. L. Saenger, G. M. McClelland, and D. R. Herschbach, J. Phys. Chem. **85**, 333 (1981).
[10] J. J. Valentini and J. B. Cross, J. Chem. Phys. **77**, 572 (1982).
[11] J. M. Philippoz, H. van den Bergh, and R. Monot, J. Phys. Chem. **91**, 2545 (1987).
[12] J. A. Beswick, R. Monot, J. M. Philippoz, and H. van den Bergh, J. Chem. Phys. **86**, 3965 (1987).
[13] M. C. R. Cockett, D. A. Beattie, R. J. Donovan, and K. P. Lawley, Chem. Phys. Lett. **259**, 554 (1996).
[14] D. A. Beattie, M. C. R. Cockett, K. P. Lawley, and R. J. Donovan, J. Chem. Soc., Faraday Trans. **93**, 4245 (1996).
[15] L. Beneventi, P. Casavecchia, and G. G. Volpi, in *Dynamics of Polyatomic van der Waals Complexes*, edited by N. Halberstadt and K. C. Janda (Plenum, New York, 1990).
[16] L. Beneventi, P. Casavecchia, G. G. Volpi, C. R. Bieler, and K. C. Janda, J. Chem. Phys. **98**, 178 (1993).
[17] A. Rohrbacher, K. C. Janda, L. Beneventi, P. Casavecchia, and G. G. Volpi, J. Phys. Chem. **101**, 6528 (1997).
[18] F.-M. Tao and W. Klemperer, J. Chem. Phys. **97**, 440 (1992).
[19] J. Sadlej, G. Chalasiński, and M. M. Szcześniak, J. Mol. Struct.: THEOCHEM **307**, 187 (1994).
[20] G. Chalasiński, M. Gutowski, M. M. Szcześniak, J. Sadlej, and S. Scheiner, J. Chem. Phys. **101**, 6800 (1994).
[21] S. M. Cybulski, R. Burcl, G. Chalasiński, and M. M. Szcześniak, J. Chem. Phys. **103**, 10116 (1995).
[22] F. Y. Naumkin and F. R. W. McCourt, J. Chem. Phys. **103**, 3392 (1995).
[23] F. Y. Naumkin and F. R. W. McCourt, Mol. Phys. **96**, 1043 (1999).
[24] A. Rohrbacher, J. Williams, K. C. Janda, S. M. Cybulski, R. Burcl, M. M. Szcześniak, G. Chalasiński, and N. Halberstadt, J. Chem. Phys. **106**, 2685 (1997).
[25] J. Williams, A. Rohrbacher, D. Djahandideh, K. C. Janda, A. Jamka, F.-M. Tao, and N. Halberstadt, Mol. Phys. **91**, 573 (1997).
[26] S. S. Huang, C. R. Bieler, K. C. Janda, F.-M. Tao, W. Klemperer, P. Casavecchia, G. G. Volpi, and N. Halberstadt, J. Chem. Phys. **102**, 8846 (1995).
[27] J. Williams, Ph.D. thesis, University of California, Irvine, 1998.
[28] C. F. Kunz, I. Burghardt, and B. A. Heß, J. Chem. Phys. **109**, 359 (1998).
[29] F. Y. Naumkin and F. R. W. McCourt, Chem. Phys. Lett. **294**, 71 (1998).
[30] F. Y. Naumkin and F. R. W. McCourt, J. Chem. Phys. **107**, 5702 (1997).
[31] F. Y. Naumkin and F. R. W. McCourt, J. Chem. Phys. **108**, 9301 (1998).
[32] F. Y. Naumkin and F. R. W. McCourt, J. Chem. Phys. **109**, 1271 (1998).
[33] F. Y. Naumkin and F. R. W. McCourt, J. Chem. Phys. **110**, 7745 (1999).
[34] J. Williams, A. Rohrbacher, J. Seong, N. Marianayagam, K. C. Janda, R. Burcl, M. M. Szcześniak, G. Chalasiński, S. M. Cybulski, and N. Halberstadt, J. Chem. Phys. **111**, 997 (1999).
[35] K. W. Chan, T. D. Power, J. Jai-nhuknan, and S. M. Cybulski, J. Chem. Phys. **110**, 860 (1999).
[36] D. G. Jahn, W. S. Barney, J. Cabalo, S. G. Clement, T. J. Slotterback, K. C. Janda, and N. Halberstadt, J. Chem. Phys. **104**, 3501 (1996).
[37] L. J. van de Burgt, J. P. Nicolai, and M. C. Heaven, J. Chem. Phys. **81**, 5514 (1984).
[38] D. G. Jahn, S. G. Clement, and K. C. Janda, J. Chem. Phys. **101**, 283 (1994).
[39] T. González-Lezana, M. I. Hernández, G. Delgado-Barrio, A. A. Buchachenko, and P. Villarreal, J. Chem. Phys. **105**, 7454 (1996).
[40] T. González-Lezana, M. I. Hernández, G. Delgado-Barrio, and P. Villarreal, J. Chem. Phys. **106**, 3216 (1997).
[41] A. Rohrbacher, T. Ruchti, K. C. Janda, A. A. Buchachenko, M. I. Hernández, T. González-Lezana, P. Villarreal, and G. Delgado-Barrio, J. Chem. Phys. **110**, 256 (1999).
[42] A. A. Buchachenko, T. González-Lezana, M. I. Hernández, M. P. De Lara Castells, G. Delgado-Barrio, and P. Villarreal, Chem. Phys. Lett. **318**, 578 (2000).
[43] A. A. Buchachenko and N. F. Stepanov, J. Chem. Phys. **104**, 9913 (1996).
[44] A. A. Buchachenko and N. F. Stepanov, J. Chem. Phys. **106**, 10134 (1997).
[45] A. A. Buchachenko and N. F. Stepanov, Russ. J. Phys. Chem. **72**, 69 (1998) (in Russian).
[46] V. S. Batista and D. F. Coker, J. Chem. Phys. **105**, 4033 (1996).
[47] B. L. Grigorenko, A. V. Nemukhin, A. A. Buchachenko, N. F. Stepanov, and S. Ya. Umanskii, J. Chem. Phys. **106**, 4575 (1997).
[48] F. Y. Naumkin, Chem. Phys. **226**, 319 (1998).
[49] J. A. Beswick and G. Delgado-Barrio, in *Structure and Dynamics of Non-Rigid Molecular Systems*, edited by Y. G. Smeyers (Kluwer, Dordrecht, 1994).

[50] A. A. Buchachenko, A. Yu. Baisogolov, and N. F. Stepanov, J. Comput. Chem. **17**, 919 (1996).
[51] J. I. Cline, B. P. Reid, D. D. Evard, N. Siwakumar, N. Halberstadt, and K. C. Janda, J. Chem. Phys. **89**, 3535 (1988).
[52] O. Roncero, J. A. Beswick, N. Halberstadt, P. Villarreal, and G. Delgado-Barrio, J. Chem. Phys. **92**, 3348 (1990).
[53] In this private communication, K. C. Janda pointed out the existence of the analytical MP4 PES based on the *ab initio* MP4 calculations by F.-M. Tao and J. Williams (Ref. 27).
[54] R. E. Smalley, L. Wharton, and D. H. Levy, J. Chem. Phys. **64**, 3266 (1976).
[55] J. A. Blazy, B. M. DeKoven, T. D. Russel, and D. H. Levy, J. Chem. Phys. **72**, 2439 (1980).
[56] D. H. Levy, Adv. Chem. Phys. **47**, 323 (1981).